energies

MDPI

Article

Effects of Volumetric Property Models on the Efficiency of a Porous Volumetric Solar Receiver

Xuewei Ni †, Tiening Liu † and Dong Liu *

School of Energy and Power Engineering, Nanjing University of Science and Technology, Nanjing 210094, China; nixuewei@njust.edu.cn (X.N.); tieningliu@163.com (T.L.)
* Correspondence: liudong15@njust.edu.cn
† These authors contributed equally to this work.

Abstract: A porous volumetric receiver is the key component in concentrated solar power systems. In this paper, we investigate the effects of volumetric parameter models on the heat collection efficiency of the volumetric receiver by numerical simulations with the combination of local thermal non-equilibrium and discrete ordinate methods. Seven volumetric convective heat transfer coefficient models and three extinction coefficient models were investigated. The efficiencies calculated using these models were compared among each other. The results show that volumetric convective heat transfer coefficient models have significant effects with a maximum difference of 27.7% in receiver efficiency for these models. Extinction coefficient models have less effects on receiver efficiency with a maximum difference of 7.3%.

Keywords: solar energy; volumetric receiver; porous media; volumetric parameter model; numerical simulation

check for updates

Citation: Ni, X.; Liu, T.; Liu, D. Effects of Volumetric Property Models on the Efficiency of a Porous Volumetric Solar Receiver. *Energies* **2022**, *15*, 3899. https://doi.org/10.3390/en15113899

Academic Editor: Tapas Mallick

Received: 22 April 2022
Accepted: 23 May 2022
Published: 25 May 2022

1. Introduction

The increasing consumption of fossil fuels and resultant emissions of greenhouse gases have received considerable attention [1]. The development and utilization of renewable energy become imminent. As a clean and renewable energy, solar energy is abundant but has low energy flux density [2]. Concentrated solar power (CSP) technology is an effective way to utilize solar energy and can replace fossil-fuel-fired thermal power generation. Rather than directly converting solar energy into electricity, CSP collects solar heat, stores it as thermal energy, and supplies the stored energy to turbines that run generators [3]. Studies have shown that with the significant improvement of CSP technology and power transmission technology, the global installed capacity is expected to reach 1000 GW by 2050, which means that CSP will cover more than 15% of global electricity demand [4]. Therefore, it will be crucial to improve the energy efficiency of CSP technology.

As a key component of CSP, the efficiency of the solar receiver has a great impact on the efficiency of CSP. Compared with conventional surface receivers, the volumetric receiver has the advantages of high heat collection efficiency and good stability [5]. For volumetric receiver, we hope to achieve the "volumetric effect" [6], i.e., the highest solid phase temperature is inside the absorber. In this way, the temperature of the front surface of the receiver can be reduced, local high temperature damage to the material can be avoided, and radiation losses can be reduced; thus, heat collection efficiency can be enhanced. Generally, porous media is considered to be a promising material as the absorber of a volumetric receiver [7]. The large specific surface area and complex pore structure of porous media not only enable it to increase the convective heat transfer between fluid and solid, but also provide a larger extinction area for the receiver to improve the temperature distribution. Therefore, using a volumetric receiver composed of porous media can achieve a higher operating temperature and minimize the radiation loss of the receiver, which helps to realize the "volumetric effect" and improve the efficiency of the receiver.

Numerous studies have presented numerical simulations of volumetric solar receivers aiming at achieving volumetric effect [8–21]. Natividade et al. [10] investigated the effects of thermal conductivity, porosity, and fluid mass flow of porous media on the solar thermal conversion efficiency of a volumetric receiver. The efficiency is expected to be as high as 85% when the fluid outlet temperature is about 950 K, but no significant "volumetric effect" was found in the study. Wang et al. [11] established a 3D theoretical model of the coupling of fluid flow and internal heat transfer, and studied the effects of porosity, pore size, volumetric heat transfer coefficient, and air flow rate on the receiver performance. In the case of porosity $\varphi = 0.95$, the thermal efficiency reached a maximum of 72.48% and the higher the φ, the more significant the "volumetric effect". From the results of the above studies, it is still not clear whether a significant volumetric effect can be achieved. The optimization results are also diverse. For example, Wang et al. [11] reported that, for porous media with the same porosity ($\varphi \sim 0.85$), the pore size decreases from 5.83 mm to 2.22 mm, and efficiency increases by nearly 3%. In contrast, Kribus et al. [16] reported that receiver efficiency increases with increasing pore size.

We believe that the inconsistence of these results is caused by the volumetric parameter models used in these studies. Porous media are often modeled as continuous translucent media, known as the continuum scale method [9]. Two important volumetric parameters are the volumetric convective heat transfer coefficient and the extinction coefficient, which have a significant impact on the internal heat transfer process and results of porous media. Many different models have been reported for these two parameters [22–30]. For example, for the volumetric convective heat transfer coefficient models, some include the length of the receiver, while some do not. The constants are also different in different extinction coefficient models. To the best of our knowledge, the effects of volumetric parameter models on the receiver efficiency have never been reported.

In this paper, we selected seven volumetric convective heat transfer coefficient models and three extinction coefficient models. The efficiency calculated using these models was compared with each other to investigate their effects on the receiver efficiency.

2. Models and Methods

Governing equations. A two-dimensional axisymmetric model was used as shown in Figure 1. The continuity and momentum equations are

$$\nabla \cdot (\rho_f \vec{V}) = 0 \tag{1}$$

$$\frac{1}{\varepsilon}\nabla\left(\rho_f \frac{\vec{V}\vec{V}}{\varphi}\right) = -\nabla P + \nabla\left(\frac{\mu_f}{\varepsilon}\nabla\vec{V}\right) + \vec{F} \tag{2}$$

where ε is the porosity. $\vec{F}$ is the momentum source term due to the porous media, and the correlation can be expressed as

$$\vec{F} = \frac{\mu_f}{k_1}\vec{V} + \frac{\rho_f}{k_2}\vec{V^2} \tag{3}$$

where k_1 is the permeability coefficient and k_2 is the inertial coefficient; the correlations are

$$k_1 = \frac{d^2}{1039 - 1002\varepsilon} \tag{4}$$

$$k_2 = \frac{d}{0.5138\varepsilon^{-5.739}} \tag{5}$$

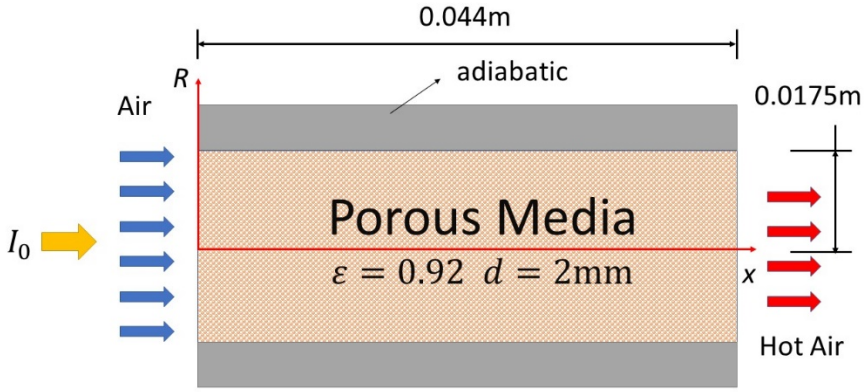

Figure 1. Schematic diagram of the porous medium solar receiver.

Volumetric convective heat transfer coefficient models. A local thermal non-equilibrium model (LTNE) was used to accurately obtain the temperature distribution of the solid and fluid. The energy equations of the fluid phase and solid phase can be defined as

$$0 = \nabla\cdot(k_{se}\nabla T_s) + h_v\left(T_f - T_s\right) - Sr \tag{6}$$

$$\nabla\cdot\left(\rho_f C_{p.f}\vec{V}T_f\right) = \nabla\cdot\left(k_{fe}\nabla T_f\right) + h_v\left(T_s - T_f\right) \tag{7}$$

where k_{fe} and k_{se} are the effective thermal conductivities of the fluid and solid phases, respectively, which are computed as $k_{fe} = \varepsilon k_f$ and $k_{se} = \frac{1}{3}(1-\varepsilon)k_s$. Sr is the source term and the correlation is:

$$Sr = k_a\left(\sum_{m=1}^{n(n+2)} I_m w_m - 4\sigma T^4\right) \tag{8}$$

In this work, we chose seven volumetric convective heat transfer coefficient models that are widely used.

Model 1:

$$Nu_l = 2.0696\varepsilon^{0.38}Re^{0.438} \tag{9}$$

$$h_v = a_{sf}Nu_l\frac{k_f}{d} \tag{10}$$

This Nusselt number model was proposed by Wu et al. [22] through simulation studies and mathematical derivation. Zhu et al. [30] applied the model in their work and gave the specific surface area formula:

$$a_{sf} = \frac{10.33H\sqrt{1-\varepsilon} - 5.8H^{1.6}(1-\varepsilon)}{d} \tag{11}$$

where $H = 1$ is defined as the Heywood circularity factor.

Model 2:

$$Nu_v = (32.504\varepsilon^{0.38} - 109.94\varepsilon^{1.38} + 166.65\varepsilon^{2.38} - 86.98\varepsilon^{3.38})Re^{0.438} \tag{12}$$

$$h_v = Nu_v\frac{k_f}{d^2} \tag{13}$$

This Nusselt number model was derived by Wu et al. [22] through mathematics.

Model 3:

$$Nu_v = \left[0.0426 + 1.236\left(\frac{d_m}{L}\right)\right]Re \tag{14}$$

where d_m is the "passage" diameter and the correlation can be defined as:

$$d_m = \sqrt{\frac{4\varepsilon}{\pi}} \tag{15}$$

This Nusselt number model was proposed by Fu et al. [23] through experimental measurements on samples of different materials, and the deviation was within ±20%.

Model 4:

$$Nu_v = 0.819\left[1 - 7.33\left(\frac{d}{L}\right)\right] Re^{0.38[1+15.5(\frac{d}{L})]} \tag{16}$$

This model was proposed by Younis [24] based on measurements on samples with porosity of 0.83–0.87 and the maximum deviation was 27.1%.

Model 5:

$$Nu_v = 1.5590 + 0.5954\mathrm{Re}^{0.5954} Pr^{0.4720} \tag{17}$$

where Pr is the Prandtl number and the correlation is:

$$Pr = \frac{C_p \mu}{k_{fe}} \tag{18}$$

This model was derived by Petrasch [25] using tomography to measure a real porous medium sample with a pore size of 2.54 mm and a porosity of 0.857.

Model 6:

$$Nu_l = 2.832 n_{PPI}^{-1.1} Re^{0.70905} \tag{19}$$

$$h_v = a_{sf} \frac{Nu_l \cdot k_f}{d_h} \tag{20}$$

$$d_h = \sqrt{(1-\varepsilon)\frac{4s^2}{3\pi}} \tag{21}$$

$$s = \frac{0.0254}{1.5 n_{PPI}} \tag{22}$$

$$a_{sf} = 35.7 n_{PPI}^{1.1461} \tag{23}$$

$$n_{PPI} = \frac{2.54 \times 10^{-2}}{d_c} \tag{24}$$

where n_{PPI} is the pore density, usually expressed by the number of pores within a length of 2.54 cm; and s is the pore diameter. This model was proposed by Xu [26]. By applying the least square method, Xu fitted the coefficients with the experimental data.

Model 7:

$$Nu_v = 0.34\varepsilon^{-2}\mathrm{Re}^{0.61} Pr^{\frac{1}{3}} \tag{25}$$

This model was proposed by Chen [27] through a large amount of experimental data fitting and applied to his subsequent work.

Extinction coefficient models. The porous media is treated as participating media, and the air is treated as transparent with a refractive index of 1 [31]. The radiative transfer equation can be expressed as:

$$\frac{\partial I_\lambda(r,\theta)}{\partial r} = -\beta I_\lambda(r,\theta) + \kappa_\alpha I_l^b[T(r)] + \frac{\sigma_\lambda}{4\pi}\int_{4\pi} \Phi(\theta' - \theta) I_\lambda(r,\theta') d\theta' \tag{26}$$

where β is the extinction coefficient, κ_α is the absorption coefficient, and σ_λ is the scattering coefficient, expressed as:

$$\beta = \kappa_\alpha + \sigma_\lambda \tag{27}$$

$$\kappa_\alpha = \alpha\beta \tag{28}$$

$$\sigma_\lambda = (1-\alpha)\beta \tag{29}$$

In this work, we selected the following extinction coefficient models:

$$\beta = \frac{C(1-\varepsilon)}{d} \tag{30}$$

This model was obtained by Hsu et al. [28] based on optical geometric analysis. In an ideal case, C = 3, and by adjusting the value of C, the model can be extended to actual porous media materials. Through comparison with the actual measured porous media material data, it was found that for SiC, C = 4.8 fitted best [29]. Therefore, the ideal cases C = 3 and C = 4.8 were used in this work.

Another extinction coefficient model was also chosen:

$$\beta = \frac{a_{sf}}{4\varepsilon} \tag{31}$$

This model was obtained by Zhu [30] through using the Monte Carlo method. In a subsequent work, Zhu verified the correctness of the model by comparing with analytical equations.

The scattering phase function for an open cell foam structure under the assumption of diffuse reflection can be expressed as

$$\Phi(\theta) = \frac{8}{3\pi}(sin\theta - \theta cos\theta) \tag{32}$$

A discrete ordinate method was used to solve the radiative transfer equation.

Boundary conditions. In this study, the concentrated solar radiation energy flow received by the front surface of the collector was set as a uniform incident energy flux of $\phi = 1.04\ \mathrm{MW/m^2}$, and the mass flow rate at the entrance was set as $0.85\ \mathrm{kg/(s{\cdot}m^2)}$. The front surface was assumed to be a pseudo-surface with a surface porosity same as the volume porosity. The lateral wall was adiabatic and the inlet air temperature was set at 300 K. The back wall was assumed to be a perfect reflector without any radiation loss, and the gauge pressure at the outlet was set as 0 Pa.

Material properties. Since the porous media solar receiver operates at high temperatures, the variations of the air physical properties with the temperature cannot be ignored during the operation of the receiver. The viscosity coefficient of air is calculated via the Sutherland law, and the expressions of air specific heat capacity and thermal conductivity are [32]:

$$C_p = 1.93 \times 10^{-10} T_f^4 - 8 \times 10^{-7} T_f^3 + 1.14 \times 10^{-3} T_f^2 - 4.49 \times 10^{-1} T_f + 1.06 \times 10^3 \tag{33}$$

$$k_f = 1.52 \times 10^{-11} T_f^3 - 4.86 \times 10^{-8} T_f^2 + 1.02 \times 10^{-4} T_f - 3.93 \times 10^{-3} \tag{34}$$

The raw material of the solid porous medium used in this paper was SiC with its specific heat capacity C_p = 750 J/(kg·K), density $\rho = 3210\ \mathrm{kg/m^3}$, and thermal conductivity $k_s = 80\ \mathrm{W/(m{\cdot}k)}$.

Numerical method. This work used the finite volume method, the SIMPLE algorithm, and the second-order upwind method to solve the governing equations. The second-order upwind method was applied to the momentum equation, energy equation, and radiation equation. The convergence criterion for all equations was set to 10^{-6}. In order to test the grid independence of the physical model, three groups of two-dimensional structured grids were established in this study. The number of elements were 8000, 16,000, and 32,000, respectively. By comparison, it is found that when the number of grids were 16,000 and 32,000, the difference between the calculated results was within 0.1%, so a structured grid with 16,000 elements was used.

Validation. This work referred to the case and data in reference [30], and compared the two-dimensional temperature distribution in the porous media region. The obtained solid region temperature contour results and the results in reference [30] are shown in Figure 2. Through comparison, it is found that the solid temperature distribution results

obtained by the two methods are very close with the temperature difference within 20 K at each position. Therefore, the model and the method in this work are reliable.

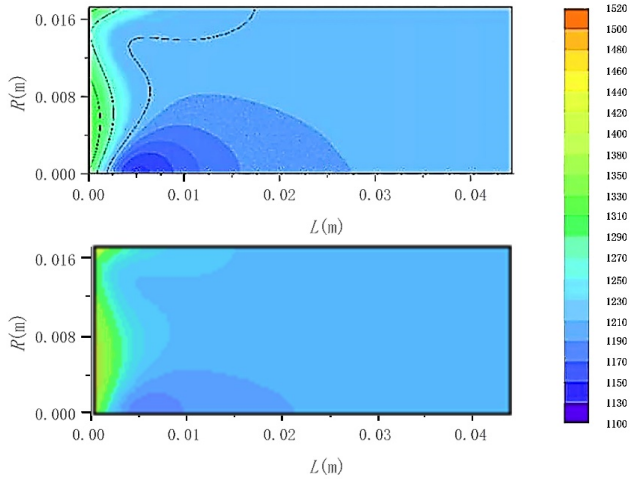

Figure 2. Comparison of the solid-phase temperature distribution between the results calculated in this work and in reference [30]. Top: reference [30]. Bottom: this work.

3. Results and Discussion

Two kinds of porous media with different parameters, $d = 2$ mm, $\varepsilon = 0.92$, $\alpha = 0.9$ and $d = 1.5$ mm, $\varepsilon = 0.8$, $\alpha = 0.95$, were used to study the effects of volumetric parameter models on the receiver efficiency. The heat collection efficiency is expressed as [33]:

$$\eta = \frac{\dot{m} \int_{T_{in}}^{T_{ex}} C_p(T) dT}{q_{in}} \tag{35}$$

where q_{in} is the solar radiation heat flux converging at the entrance of the receiver, W/m^2; m is the mass flow rate per unit area, kg/(s·m^2); T_{in} and T_{ex} are the fluid temperatures at the inlet and outlet of the receiver, K, respectively.

The first porous media. Figures 3 and 4 are graphs of the temperature distributions along the receiver axis obtained by using different volumetric convective heat transfer coefficient models when the extinction coefficient model is Equation (30) and C = 3 and 4.8, respectively. The corresponding heat collection efficiencies are shown in Tables 1 and 2.

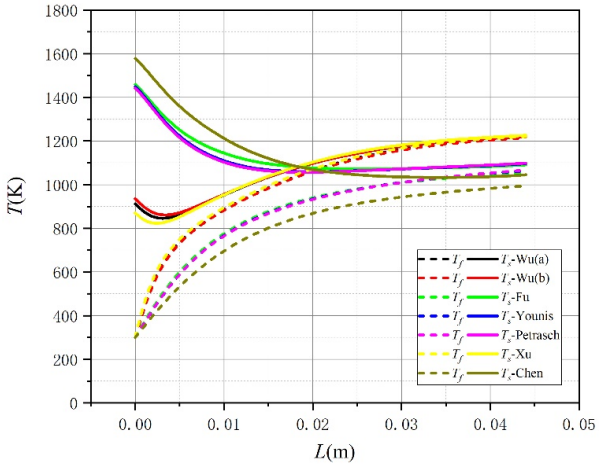

Figure 3. Material 1: temperature distributions with various volumetric convective heat transfer coefficient models when C = 3.

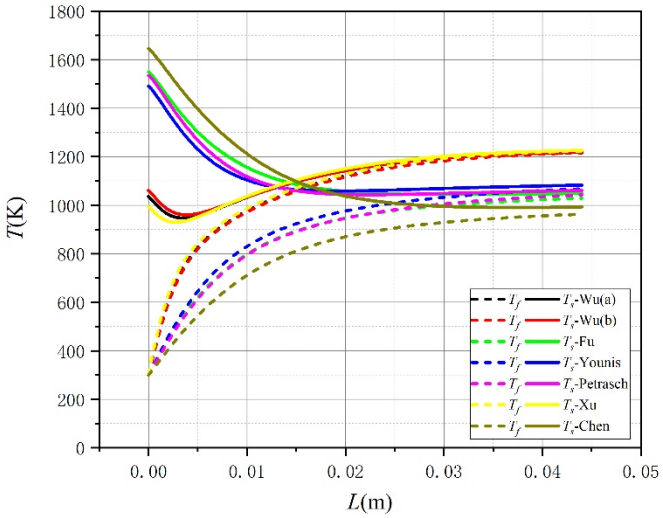

Figure 4. Material 1: temperature distributions with various volumetric convective heat transfer coefficient models when C = 4.8.

Table 1. Material 1: heat collection efficiency for different volumetric convective heat transfer coefficient models when C = 3.

Model	Wu(a)	Wu(b)	Fu	Younis	Petrasch	Xu	Chen
Efficiency	0.821	0.817	0.663	0.675	0.673	0.824	0.606

Table 2. Material 1: heat collection efficiency under different volumetric convective heat transfer coefficient models when C = 4.8.

Model	Wu(a)	Wu(b)	Fu	Younis	Petrasch	Xu	Chen
Efficiency	0.819	0.815	0.638	0.671	0.651	0.821	0.577

As can be seen from Figure 3, when the extinction model is used as Equation (30) with C = 3, the simulation results obtained by different volumetric convective heat transfer coefficient models are quite different. When models 1, 2, and 6 are used, heat transfer is more efficient and the so-called volumetric effect is achieved; thus, the heat collection efficiency corresponding to the three volumetric convective heat transfer coefficient models is higher than that for other models. According to Table 2, it can be found that different volumetric convective heat transfer coefficient models lead to a large difference in the heat collection efficiency of the receiver. The efficiency of model 6 is the highest and the efficiency corresponding to model 7 is the lowest; the difference between the two is 21.8%.

It can be seen from Figure 4 that when the extinction model is used as Equation (30) with C = 4.8, the simulation results obtained by different volumetric convective heat transfer coefficient models are also very different. When models 1, 2, and 6 are selected, heat transfer inside the receiver is also more efficient and the volumetric effect can be achieved. The heat collection efficiency obtained by using different volumetric convective heat transfer coefficient models is shown in Table 2. The heat collection efficiency is quite different under the influence of different models. The heat collection efficiency corresponding to models 1, 2, and 6 is higher compared to other volumetric convective heat transfer coefficient model. The efficiency corresponding to model 6 is the highest and the efficiency obtained by using model 7 is the lowest; the difference between the two is 24.4%.

By comparing Tables 1 and 2, it is found that the selection of different C, that is, the selection of different extinction coefficient models, has less effect on the heat collection efficiency of the receiver. However, when C = 3, the heat collection efficiency obtained by using different volumetric convective heat transfer coefficient models is slightly higher than that when C = 4.8. This is because a smaller C means a smaller extinction coefficient

and thereby, the extinction area of the porous medium becomes larger. Thus, the solar radiation absorbed by the front end of the receiver decreases and as a result, the front-end temperature decreases. Consequently, the radiation loss is reduced and the heat collection efficiency is increased.

Figure 5 shows the temperature distribution of the receiver axis obtained by simulating seven different volumetric convective heat transfer coefficient models when the porous medium material 1 is selected and the extinction coefficient model is Equation (31). The corresponding heat collection efficiency is shown in Table 3; when model 6 is selected, the efficiency is the highest and model 7 is the lowest; the difference between the two is 27.7%. The heat collection efficiency for the extinction coefficient model in Equation (31) is lower than that for the model in Equation (30).

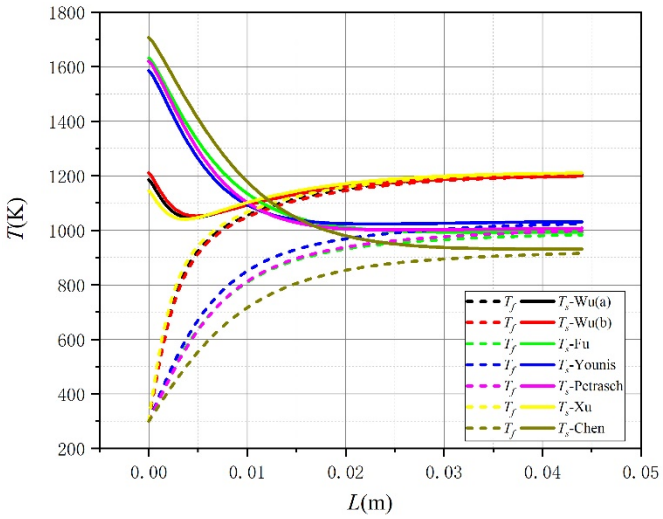

Figure 5. Material 1: temperature distributions with various volumetric convective heat transfer coefficient models when using Equation (31).

Table 3. Material 1: heat collection efficiency under different volumetric convective heat transfer coefficient models when using Equation (31).

Model	Wu(a)	Wu(b)	Fu	Younis	Petrasch	Xu	Chen
Efficiency	0.805	0.799	0.596	0.634	0.609	0.810	0.533

Based on the above three simulation results, when the porous medium material is selected as $d = 2$ mm, $\varepsilon = 0.92$, $\alpha = 0.9$, the selection of different extinction coefficient models has less effect on the heat collection efficiency, while the selection of different volumetric convective heat transfer coefficient models has a greater impact on the simulation results. When the volumetric convective heat transfer coefficient models 1, 2, and 6 are selected, heat transfer is more efficient and the heat collection efficiency of the receiver is higher than that for other models. When the volumetric convective heat transfer coefficient model 7 is selected, the efficiency difference can reach a maximum of 7.3% between the results for the ideal extinction coefficient model and the extinction coefficient model in Equation (31). When the extinction coefficient model in Equation (31) is selected, the maximum difference is 27.7% between the efficiency calculated using volumetric convective heat transfer coefficient models 6 and 7.

The second porous media. Figures 6 and 7 show the temperature distributions along the receiver axis obtained by simulating different volumetric convective heat transfer coefficient models when the extinction coefficient model is selected as Equation (30) and C = 3 and 4.8. Tables 4 and 5 are the corresponding receiver heat collection efficiency. From Figures 6 and 7, we find that, for material 2 using the extinction coefficient model Equation (30), the simulation results obtained by different volumetric convective heat

transfer coefficient models are quite different, regardless of whether *C* is 3 or 4.8. When models 1 and 2 are selected, the highest temperature appears inside the porous medium to achieve the volumetric effect, and the corresponding heat collection efficiency is also higher compared to other models. With the change of the basic parameters of the porous medium, the highest temperature of the solid skeleton appears at the front end of the receiver when using model 6 and the volumetric effect no longer appears. This is because the reduction in the porosity and pore size leads to the enhancement of the extinction ability of the porous medium material; thus, the front end of the receiver receives more solar radiation resulting in increased temperature of the front surface and more re-radiation losses. Consequently, heat collection efficiency decreases.

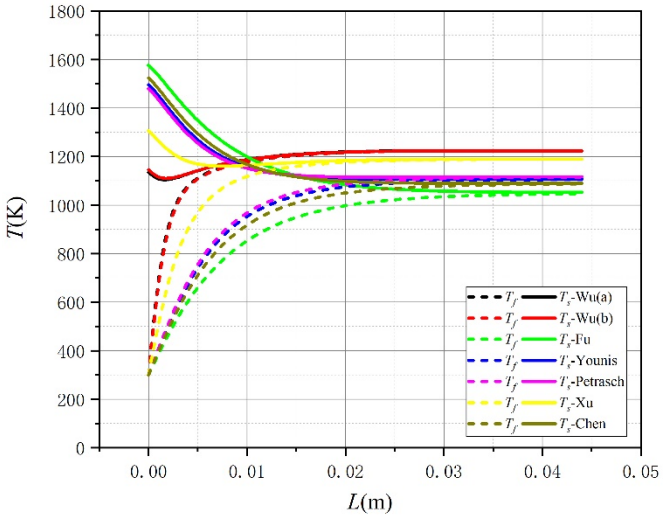

Figure 6. Material 2: temperature distributions with various volumetric convective heat transfer coefficient models when *C* = 3.

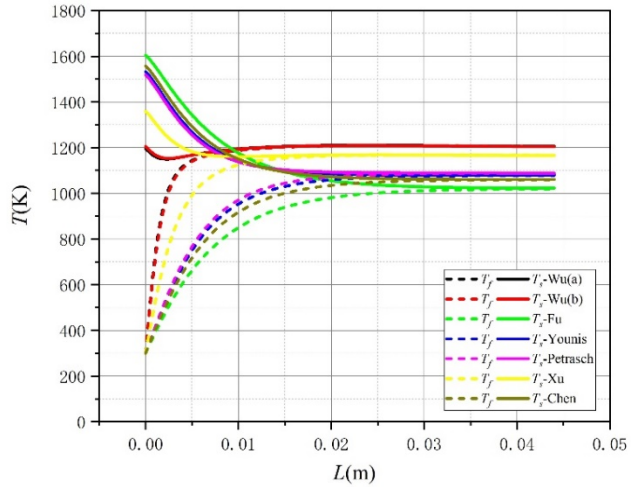

Figure 7. Material 2: temperature distributions with various volumetric convective heat transfer coefficient models when *C* = 4.8.

Table 4. Material 2: heat collection efficiency under different volumetric convective heat transfer coefficient models when *C* = 3.

Model	Wu(a)	Wu(b)	Fu	Younis	Petrasch	Xu	Chen
Efficiency	0.823	0.823	0.655	0.711	0.720	0.791	0.693

Table 5. Material 2: heat collection efficiency under different volumetric convective heat transfer coefficient models when C = 4.8.

Model	Wu(a)	Wu(b)	Fu	Younis	Petrasch	Xu	Chen
Efficiency	0.806	0.805	0.629	0.685	0.694	0.768	0.667

Figure 8 shows the temperature distributions along the receiver axis obtained by the simulations of different volumetric convective heat transfer coefficient models when the porous medium material 2 is selected and the extinction coefficient model is Equation (31). The corresponding heat collection efficiency is shown in Table 6. Compared with the above results obtained with different extinction coefficient models, it is found that the volumetric convective heat transfer coefficient models 1 and 2 can still achieve a more significant volumetric effect, so the receiver has a higher heat collection efficiency.

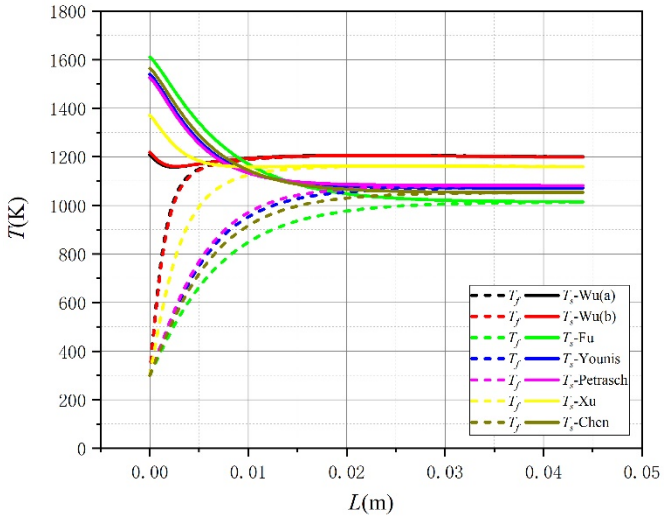

Figure 8. Material 2: temperature distributions with various volumetric convective heat transfer coefficient models when using Equation (31).

Table 6. Material 2: heat collection efficiency under different volumetric convective heat transfer coefficient models when using Equation (31).

Model	Wu(a)	Wu(b)	Fu	Younis	Petrasch	Xu	Chen
Efficiency	0.801	0.800	0.623	0.678	0.688	0.762	0.661

4. Conclusions

This paper investigated the effects of volumetric parameter models on the performance of porous volumetric solar receivers. From the view of convection and radiation heat transfer, which are difficult to grasp and analyze in porous media, numerical simulations were carried out for various volumetric convective heat transfer coefficient models and extinction coefficient models to obtain the temperature distributions inside the receiver and the corresponding heat collection efficiency. The results calculated using these models were compared with each other. Conclusions and outlooks are as follows.

(1) Volumetric convective heat transfer coefficient models have a greater impact on the numerical simulation results, while the extinction coefficient model has less effect on the overall simulation results. Using different extinction coefficient models results in an efficiency difference of up to 7.3%, while using different volumetric convective heat transfer coefficient models results in a much larger difference of up to 27.7%.

(2) These significant performance differences from various volumetric parameter models show that further studies are highly needed to determine or to obtain accurate models for porous volumetric solar receivers before we can trust any optimization results. Currently, it is hard to tell which model is more accurate.

Author Contributions: Formal analysis, X.N.; Methodology, T.L.; Supervision, D.L.; Writing—original draft, X.N. and T.L.; Writing—review and editing, D.L. All authors have read and agreed to the published version of the manuscript.

Funding: This work was supported by the National Key R&D Program of China (No. 2021YFF0500700) and the Natural Science Foundation of Jiangsu Province (No. BK20200072).

Informed Consent Statement: Not applicable.

Data Availability Statement: The data presented in this study are available on request from the corresponding author.

Conflicts of Interest: The authors declare no conflict of interest.

References

1. Koçak, B.; Fernandez, A.I.; Paksoy, H. Review on sensible thermal energy storage for industrial solar applications and sustainability aspects. *Sol. Energy* **2020**, *209*, 135–169. [CrossRef]
2. Ruidong, W.; Jun, M.A. Status and Future Development Prospects of CSP. *IOP Conf. Ser. Earth Environ. Sci.* **2021**, *687*, 012088. [CrossRef]
3. Feng, C.; Shao, C.; Wang, X. CSP clustering in unit commitment for power system production cost modeling. *Renew. Energy* **2021**, *168*, 1217–1228. [CrossRef]
4. Viebahn, P.; Lechon, Y.; Trieb, F. The potential role of concentrated solar power (CSP) in Africa and Europe—A dynamic assessment of technology development, cost development and life cycle inventories until 2050. *Energy Policy* **2011**, *39*, 4420–4430. [CrossRef]
5. Ávila-Marín, A.L. Volumetric receivers in Solar Thermal Power Plants with Central Receiver System technology: A review. *Sol. Energy* **2011**, *85*, 891–910. [CrossRef]
6. Weinstein, L.A.; Loomis, J.; Bhatia, B.; Bierman, D.M.; Wang, E.N.; Chen, G. Concentrating Solar Power. *Chem. Rev.* **2015**, *115*, 12797–12838. [CrossRef]
7. Fend, T.; Hoffschmidt, B.; Pitz-Paal, R.; Reutter, O.; Rietbrock, P. Porous materials as open volumetric solar receivers: Experimental determination of thermophysical and heat transfer properties. *Energy* **2004**, *29*, 823–833. [CrossRef]
8. Andreozzi, A.; Bianco, N.; Iasiello, M.; Naso, V. Thermo-Fluid-Dynamics of a Ceramic Foam Solar Receiver: A Parametric Analysis. *Heat Transf. Eng.* **2019**, *41*, 1085–1099. [CrossRef]
9. Barreto, G.; Canhoto, P.; Collares-Pereira, M. Parametric analysis and optimisation of porous volumetric solar receivers made of open-cell SiC ceramic foam. *Energy* **2020**, *200*, 117476. [CrossRef]
10. Natividade, J. Parametric Study of High-Temperature Volumetric Solar Absorbers. Master's Thesis, Universidade de Lisboa—Instituto Superior Técnico, Lisbon, Portugal, 2015.
11. Wang, P.; Li, J.B.; Xu, R.N.; Jiang, P.X. Non-uniform and volumetric effect on the hydrodynamic and thermal characteristic in a unit solar absorber. *Energy* **2021**, *225*, 120130. [CrossRef]
12. Barreto, G.; Canhoto, P.; Collares-Pereira, M. Three-dimensional modelling and analysis of solar radiation absorption in porous volumetric receivers. *Appl. Energy* **2018**, *215*, 602–614. [CrossRef]
13. Navalho, J.E.P.; Pereira, J.C.F. A comprehensive and fully predictive discrete methodology for volumetric solar receivers: Application to a functional parabolic dish solar collector system. *Appl. Energy* **2020**, *267*, 114781. [CrossRef]
14. Ren, Y.; Qi, H.; Shi, J.; Chen, Q.; Wang, Y.; Ruan, L. Thermal Performance Characteristics of Porous Media Receiver Exposed to Concentrated Solar Radiation. *J. Energy Eng.* **2017**, *143*, 04017013. [CrossRef]
15. Chen, X.; Xia, X.-L.; Yan, X.-W.; Sun, C. Heat transfer analysis of a volumetric solar receiver with composite porous structure. *Energy Convers. Manag.* **2017**, *136*, 262–269. [CrossRef]
16. Kribus, A.; Gray, Y.; Grijnevich, M.; Mittelman, G.; Mey-Cloutier, S.; Caliot, C. The promise and challenge of solar volumetric absorbers. *Sol. Energy* **2014**, *110*, 463–481. [CrossRef]
17. Godini, A.; Kheradmand, S. Optimization of volumetric solar receiver geometry and porous media specifications. *Renew. Energy* **2021**, *172*, 574–581. [CrossRef]
18. Zhu, Q.; Xuan, Y. Improving the performance of volumetric solar receivers with a spectrally selective gradual structure and swirling characteristics. *Energy* **2019**, *172*, 467–476. [CrossRef]
19. Xie, T.; Xu, K.; Yang, B.; He, Y. Effect of pore size and porosity distribution on radiation absorption and thermal performance of porous solar energy absorber. *Sci. China Technol. Sci.* **2019**, *62*, 2213–2225. [CrossRef]

20. Du, S.; Li, Z.; He, Y.-L.; Li, D.H.; Xie, X.; Gao, Y. Experimental and numerical analysis of the hydraulic and thermal performances of the gradually-varied porous volumetric solar receiver. *Sci. China Technol. Sci.* **2020**, *63*, 1224–1234. [CrossRef]
21. Barreto, G.; Canhoto, P.; Collares-Pereira, M. Combined experimental and numerical determination of the asymmetry factor of scattering phase functions in porous volumetric solar receivers. *Sol. Energy Mater. Sol. Cells* **2020**, *206*, 110327. [CrossRef]
22. Wu, Z.; Caliot, C.; Flamant, G.; Wang, Z. Numerical simulation of convective heat transfer between air flow and ceramic foams to optimise volumetric solar air receiver performances. *Int. J. Heat Mass Transf.* **2011**, *54*, 1527–1537. [CrossRef]
23. Viskanta, X.F.R.; Gore, J.P. Measurement and correlation of volumetric heat transfer coefficients of cellular ceramics. *Exp. Therm. Fluid Sci.* **1998**, *17*, 285–293. [CrossRef]
24. Younis, L.; Viskanta, R. Experimental determination of the volumetric heat transfer coefficient between stream of air and ceramic foam. *Int. J. Heat Mass Transf.* **1993**, *36*, 1425–1434. [CrossRef]
25. Petrasch, J.; Wyss, P.; Steinfeld, A. Tomography-based Monte Carlo determination of radiative properties of reticulate porous ceramics. *J. Quant. Spectrosc. Radiat. Transf.* **2007**, *105*, 180–197. [CrossRef]
26. Chang, X.; De-You, L.; Yuan, Z.; Su, G.; Yan, Y. Unsteady Heat Transfer of Porous Media Solar Receiver. *J. S. China Univ. Technol. (Nat. Sci. Ed.)* **2011**, *39*, 42, 46, 51.
27. Xue, C. Investigation on Forced Convection and Coupled Heat Transfer with High Temperature Radiation in Cellular Porous Material. Ph.D. Thesis, Harbin Institute of Technology, Harbin, China, 2016.
28. Hsu, P.-F.; Howell, J.R. Measurements of thermal conductivity and optical properties of porous partially stabilized zirconia. *Exp. Heat Transf.* **1992**, *5*, 293–313. [CrossRef]
29. Hendricks, T.J.; Howell, J.R. Absorption/Scattering Coefficients and Scattering Phase Functions in Reticulated Porous Ceramics. *J. Heat Transf.* **1996**, *118*, 79–87. [CrossRef]
30. Zhu, Q.; Xuan, Y. Performance analysis of a volumetric receiver composed of packed shaped particles with spectrally dependent emissivity. *Int. J. Heat Mass Transf.* **2018**, *122*, 421–431. [CrossRef]
31. Cunsolo, S.; Oliviero, M.; Harris, W.M.; Andreozzi, A.; Bianco, N.; Chiu, W.K.S.; Naso, V. Monte Carlo determination of radiative properties of metal foams: Comparison between idealized and real cell structures. *Int. J. Therm. Sci.* **2015**, *87*, 94–102. [CrossRef]
32. Mulholland, G.W. Smoke production and properties. In *SFPE Handbook of Fire Protection Engineering*; National Fire Protection Association: Quincy, MA, USA, 1995; Chapter 30; pp. 217–227.
33. Aichmayer, L.; Garrido, J.; Wang, W.; Laumert, B. Experimental evaluation of a novel solar receiver for a micro gas-turbine based solar dish system in the KTH high-flux solar simulator. *Energy* **2018**, *159*, 184–195. [CrossRef]